Journal of Materials Chemistry C

RSC Publishing

PAPER

View Article Online
View Journal

Spin orientation transition across the single-layer graphene/nickel thin film interface

Cite this: DOI: 10.1039/c3tc30872c

Yoshihiro Matsumoto,*[a] Shiro Entani,[a] Akihiro Koide,[b] Manabu Ohtomo,[a] Pavel V. Avramov,[a] Hiroshi Naramoto,[a] Kenta Amemiya,[c] Takashi Fujikawa[b] and Seiji Sakai[a]

Received 9th May 2013
Accepted 8th July 2013

DOI: 10.1039/c3tc30872c

www.rsc.org/MaterialsC

The spin-polarized electronic structures across the interface between single-layer graphene and a Ni(111) thin film are explored by employing depth-resolved X-ray absorption and magnetic circular dichroism spectroscopy with atomic layer resolution. The depth-resolved Ni $L_{2,3}$-edge analysis clarifies that the Ni atomic layers adjacent to the interface show a transition of the spin orientation to the perpendicular one in contrast to the in-plane one in the bulk region. The C *K*-edge analysis reveals the intensification of the spin–orbit interactions induced by the π–d hybridization at the interface as well as out-of-plane spin polarization in the π band region of graphene. The present study indicates the importance of the interface design at the atomic layer level for graphene-based spintronics.

Introduction

Graphene-based spintronics is a very active research area because of the great potential of graphene for spin transport as represented by the long spin-diffusion length, extremely high carrier mobility and electronic tunability.[1,2] Information on the spin-polarized electronic structures of the graphene/ferromagnetic metal (FM) interfaces is of special importance for the development of graphene-based spintronics because spin injection and detection by the use of magnetic electrodes are essential for spin valve devices. The theoretical study has provided a promising feature for spin injection through the graphene/FM interface; that is, the graphene on FMs (Ni and Co) could serve as a perfect spin filter considering the energy band dispersion of graphene relative to that of bulk FM.[3] However, despite the intensive efforts to develop the graphene spin valve devices,[2,4–7] the problem of the low spin injection efficiency *via* the graphene/FM interfaces has not been resolved yet. Recently, the spectroscopic approaches have begun to shed light on the spin-polarized electronic structures of the graphene/FM interfaces. In particular, the approaches employing X-ray absorption (XAS) and magnetic circular dichroism (XMCD) spectroscopies have suggested a significant modification of the electronic structures and spin states of graphene at the graphene/FM interface.[8] An innovative approach which can provide information across the regions both on the metal and graphene sides is required for the full understanding of the spin-polarized electronic structures of the graphene/FM interface, which would allow us to understand the underlying reasons for the low spin injection efficiency and also to control that in graphene devices.

In the present study, we apply the depth-resolved XAS and XMCD techniques[9,10] with subnanometer depth-resolution to the bilayer structure of single-layer graphene (SLG) and a Ni(111) thin film. By analyzing XAS and XMCD spectra at the Ni $L_{2,3}$-edge as a function of the mean probing depth (λ_p) from the graphene/Ni(111) interface and those at the C *K*-edge, it is successfully shown that the graphene/Ni(111) interface favours the perpendicular magnetic anisotropy (PMA), and the SLG/Ni(111) thin film undergoes a transition of the spin orientation from "in-plane" to "out-of-plane" across the interface.

Experimental

The bilayer-structured SLG/Ni(111) thin film was obtained by the ultrahigh vacuum chemical vapour deposition (UHV-CVD) technique in a molecular beam epitaxy (MBE) chamber with a base pressure of 3×10^{-7} Pa. Firstly, an atomically flat 30 nm thick Ni(111) film was prepared on an atomically flat α-Al_2O_3(0001) substrate by deposition at 423 K and post-annealing at 873 K. Subsequently, SLG was epitaxially grown on the Ni(111) surface by exposing to 100 langmuir of benzene (C_6H_6) at the substrate temperature of 873 K. Ni (99.99% purity) was deposited by using an electron beam evaporator, and benzene was introduced into the MBE chamber after purification by repeating the freeze–pump–thaw cycle several times. The partial pressure of benzene was kept at 10^{-5} Pa during the SLG growth. Highly uniform SLG with complete surface coverage can be

[a]*Advanced Science Research Center, Japan Atomic Energy Agency, 2-4 Shirakata-Shirane, Tokai, Naka, 319-1195, Japan. E-mail: matsumoto.yoshihiro@jaea.go.jp*

[b]*Graduate School of Advanced Integration Science, Chiba University, 1-33 Yayoi-cho, Inage-ku, Chiba, 263-8522, Japan*

[c]*Institute of Materials Structure Science, High Energy Accelerator Research Organization(KEK), 1-1 Oho, Tsukuba, 305-0801, Japan*

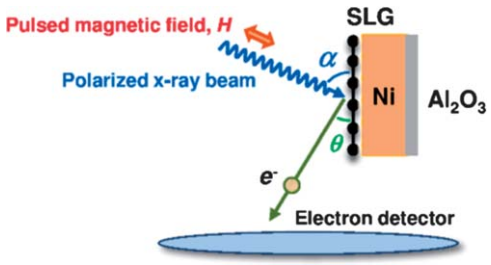

Fig. 1 The schematic representation of the set-up of the XAS and XMCD measurements.

synthesized under these preparation conditions, as has been shown in the previous study.[11]

The XAS and XMCD measurements were performed at the soft X-ray beam line BL-7A at the Photon Factory, KEK (Tsukuba, Japan). The XMCD chamber is equipped with an electromagnet and an imaging type electron detector, which is composed of a phosphor screen, a micro-channel plate and a retarding grid for collecting Auger electrons selectively, for the depth-resolved measurements. The XMCD chamber was maintained at a pressure of 7×10^{-7} Pa during the measurements. The samples prepared in the MBE chamber were transferred into the XMCD chamber without breaking the vacuum. The C *K*-edge and Ni $L_{2,3}$-edge measurements with the linearly and circularly polarized X-ray beams (the circular polarization factor, P_c, was 0.8) were performed at room temperature in the partial-electron-yield (PEY) mode by collecting Auger electrons at retarding voltages of 150 V and 500 V, respectively. The schematic representation of the experimental set-up is given in Fig. 1.

The linearly and circularly polarized X-ray beams were irradiated on the SLG/Ni(111) thin film at the incidence angle α with respect to the sample surface. The incidence angle was varied in the range of α = 20–90° to analyse the structure and the spin orientation (see below). Auger electrons emitted in the sample were detected using the imaging type electron detector. Since the escape depth of the emitted electrons changes depending on the emitting angle, the mean probing depth λ_p can be estimated from the edge-jump intensity at the detection angle θ between the sample surface and the area on the detector.[9,10] The depth-resolved and non-depth-resolved (PEY for simplicity) XAS and XMCD spectra were taken at θ = 3–30° as the sum of the signals in the relevant angle range, respectively. The XMCD measurements were performed in remanence by applying the pulsed magnetic field ($H = \pm 1600$ Oe, a pulse duration <1 s) parallel (μ^+) and antiparallel (μ^-) to the propagation direction of the circularly polarized X-ray beam with α. The XMCD spectra, which provide information on the magnetic moments along α, were obtained by taking the difference of the XAS signals ($\Delta\mu = \mu^+ - \mu^-$). It was confirmed that the Ni(111) thin film in the sample has an in-plane easy axis of magnetization by using a SQUID magnetometer after the XAS and XMCD measurements.

Results and discussions

Fig. 2a and b show the PEY C *K*-edge and Ni $L_{2,3}$-edge XAS spectra of the SLG/Ni(111) thin film as a function of the incidence angle

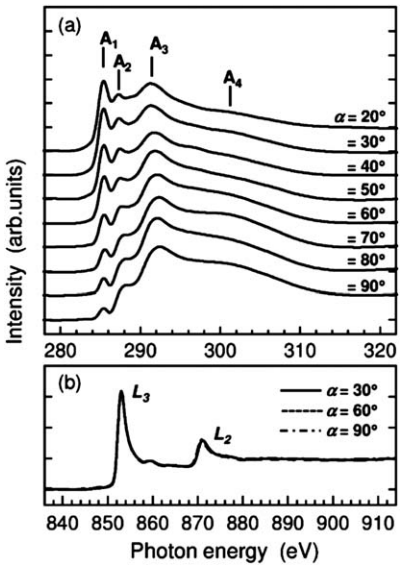

Fig. 2 The PEY (a) C *K*-edge and (b) Ni $L_{2,3}$-edge XAS spectra obtained at different incidence angles α measured with the linearly polarized X-ray beam.

α, respectively. The spectra were obtained with the linearly polarized beam. Four prominent peaks labelled as A_1, A_2, A_3 and A_4 are observed in Fig. 2a in consistency with the previously reported results.[12–15] The A_1 (285.5 eV) and A_2 (287.4 eV) peaks show strong α dependence; the A_1 and A_2 peaks increase in their intensities at a grazing incidence with a larger projection of the electric field vector of X-rays normal to the film surface, and decrease fairly at the normal incidence ($\alpha = 90°$). Meanwhile, the A_3 (292.5 eV) and A_4 (301 eV) peaks show the weak intensity dependence on α. The A_1 and A_2 peaks are due to the excitations from the 1s states to the hybridized states between the π^* (p_z) states around the *K*- and *M*-points of graphene and the Ni 3d states, respectively. The A_3 and A_4 peaks are attributed to the excitations to the σ^* states around the *Γ*- and *K*-points of graphene, respectively. Additionally, two weak shoulder components are recognized around 284 eV and 289 eV. The former and the latter can be attributed to the excitations to the localized states introduced by defects and by C–H bonds, respectively.[16,17] In Fig. 2b, the L_3 and L_2 peaks are located at 852 eV and 871 eV, which is consistent with the result of pure Ni. The satellite peak located at 6 eV higher photon energy than the L_3 peak is attributed to the multiple scattering effect in fcc Ni.[18]

Fig. 3 shows the depth-resolved Ni $L_{2,3}$-edge XAS and XMCD spectra obtained at different incidence angles (α = 30°: left panels and α = 60°: right panels) and detection angles (θ = 3°: blue lines and θ = 30°: red lines) with the circularly polarized beam. The XAS spectra represent the averaged quantities of μ^+ and μ^-.

As the detection angle θ decreases, the mean probing depth decreases and thus the relative fraction of the signals from the Ni atomic layer near the graphene/Ni(111) interface increases. The shapes of the Ni $L_{2,3}$-edge XAS spectra at θ = 3° and 30° are consistent with each other for both α, suggesting that the crystallinity of Ni is kept even in the vicinity of the interface. This can be associated with the small lattice mismatch (1%)

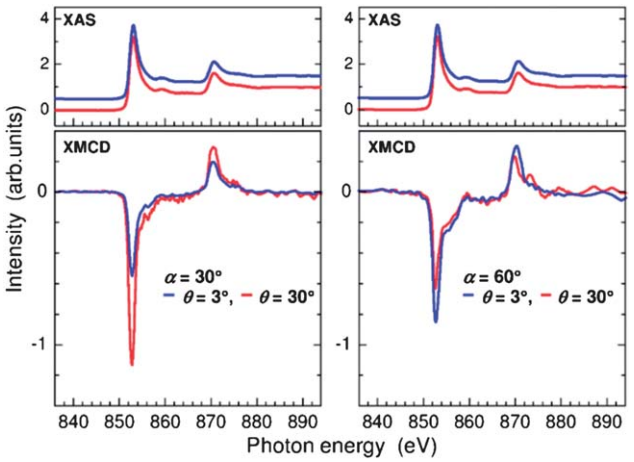

Fig. 3 The depth-resolved Ni $L_{2,3}$-edge XAS and XMCD spectra at the incidence angles of $\alpha = 30°$ (left panels) and $\alpha = 60°$ (right panels). The spectra were measured in remanence with the circularly polarized beam. The blue and red lines in the spectra represent the data at the detection angles of $\theta = 3°$ and $\theta = 30°$, respectively. The XAS spectra in the top panels are offset vertically for clarity.

between graphene and Ni(111). The decrease of the detection angle from $\theta = 30°$ (red lines) to $\theta = 3°$ (blue lines) leads to the decrease and the increase of the XMCD intensity at $\alpha = 30°$ and $\alpha = 60°$, respectively. This behaviour indicates that the spin-polarized electronic structures of the Ni(111) thin film change depending on the distance from the graphene/Ni(111) interface.

To explore the depth-dependent change in more detail, the effective spin and orbital magnetic moments of Ni in the direction parallel to α ($M^{\mathrm{eff}}_{\mathrm{spin}}(\alpha)$ and $M_{\mathrm{orb}}(\alpha)$) are calculated for the data at $\alpha = 30°$ and $\alpha = 60°$ in the range of $\theta = 3$–$30°$ by applying the XMCD sum rules.[19,20] Fig. 4 shows $M^{\mathrm{eff}}_{\mathrm{spin}}(\alpha)$ and

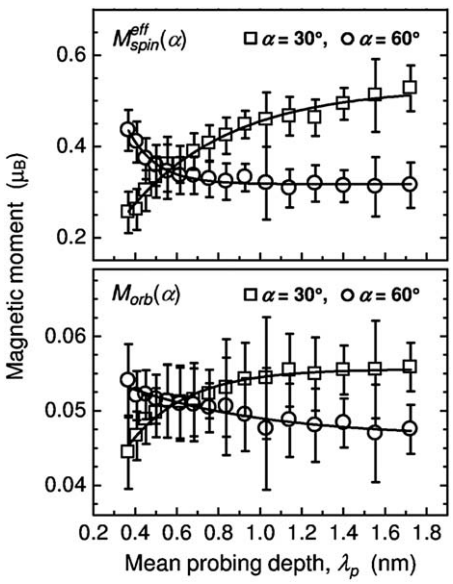

Fig. 4 The mean probing depth λ_p dependences of the effective spin moment (upper panel) and the orbital magnetic moment (lower panel) parallel to the directions of $\alpha = 30°$ (squares) and $\alpha = 60°$ (circles), respectively. The solid curves are guides for eyes.

$M_{\mathrm{orb}}(\alpha)$ ($\alpha = 30°$ and $\alpha = 60°$) as a function of the mean probing depth λ_p.

It is found that $M^{\mathrm{eff}}_{\mathrm{spin}}(\alpha)$ and $M_{\mathrm{orb}}(\alpha)$ at $\alpha = 30°$ and $\alpha = 60°$ exhibit contrasting changes depending on λ_p. At the sufficiently larger λ_p than 1 nm, both $M^{\mathrm{eff}}_{\mathrm{spin}}(\alpha)$ and $M_{\mathrm{orb}}(\alpha)$ along $\alpha = 30°$ are remarkably large compared to those along $\alpha = 60°$. However, in the range of $\lambda_p < \sim 1$ nm, the moments along $\alpha = 30°$ and $\alpha = 60°$ show decreasing and increasing tendencies with decreasing λ_p, respectively. The above analysis deduces the λ_p-dependent changes of the total magnetic moment M_{total} and its direction γ (the angle from the in-plane direction), which is described by the following equation;

$$M'_{\mathrm{total}}(\alpha) = M_{\mathrm{total}}\cos(\alpha - \gamma),$$

where

$$M'_{\mathrm{total}}(\alpha) = M^{\mathrm{eff}}_{\mathrm{spin}}(\alpha) + M_{\mathrm{orb}}(\alpha).$$

By solving the equation for $M^{\mathrm{eff}}_{\mathrm{spin}}(\alpha)$ and $M_{\mathrm{orb}}(\alpha)$ at $\alpha = 30°$ and 60°, it is obtained that $M_{\mathrm{total}} = 0.55\ \mu_B$ and $\gamma = 87°$ for the Ni atomic layers adjacent to the interface (*i.e.*, $\lambda_p = 0.4$ nm) and $M_{\mathrm{total}} = 0.66\ \mu_B$ and $\gamma = 3°$ for the region distant from the interface (*i.e.*, $\lambda_p \sim 1.7$ nm), respectively. For the latter, M_{total} agrees well with that of bulk Ni,[21] and the small deviation of γ from the in-plane direction ($\gamma = 90°$) can be attributed to the signal contribution from the shallower region with larger γ. The above results clearly demonstrate that, in the Ni atomic layers within 1 nm distance from the interface, there appears a continuous change of the spin polarization direction from in-plane to out-of-plane toward the interface, along with the decrease of the total magnetic moment by about 20%. It is reasonable to say that the graphene/Ni(111) interface strongly favours PMA as it can work against the magnetization direction of the Ni(111) thin film. It is worthy to note that the extent of the magnetic moment decrease agrees well with the theoretically estimated values for the first to the third Ni atomic layer from the graphene/Ni(111) interface under the so-called top-fcc configuration where the C atoms belonging to the two different sub-lattices are located above the first and the third Ni atomic layers.[22–24]

Fig. 5 shows the PEY C *K*-edge XAS and XMCD spectra obtained at $\alpha = 30°$ and $\alpha = 60°$, respectively. Large XMCD signals are observed around 285 eV which roughly corresponds to the A_1 peak position. Small but non-negligible XMCD signals are also observed around 291 eV near the A_3 peak position.

Due to the absence of the spin–orbit interactions (SOI) in the 1s initial states, the C *K*-edge XMCD is expected to reflect only the orbital magnetic moment of the 2p states.[25] Not only the spin polarization but also the significant enhancement of SOI should be considered in order to explain the large XMCD signals near the A_1 peak position because the intrinsic SOI strength around the *K*-point of pristine graphene[26,27] is too small to generate the orbital magnetic moment so as to detect the XMCD signals. The magnetic edge states of graphene can also contribute to the XAS and XMCD signals. However, the signals due to the edge states should be detected around 284 eV,[28]

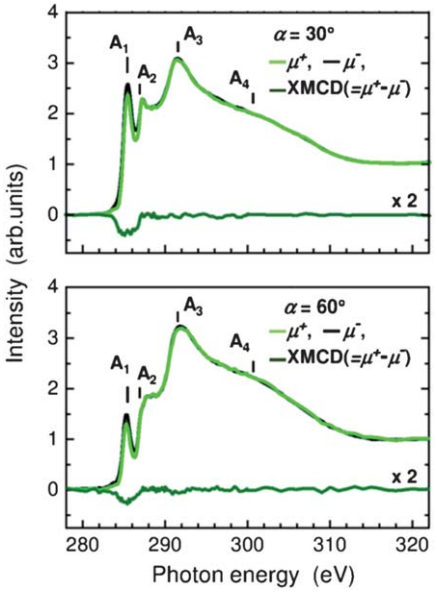

Fig. 5 The PEY C *K*-edge XAS spectra (μ^+ and μ^-) and XMCD spectra ($\Delta\mu = \mu^+ - \mu^-$) indicated by the black, light green and dark green lines at the incidence angles $\alpha = 30°$ (top panel) and $\alpha = 60°$ (bottom panel), respectively. The spectra were measured in remanence with the circularly polarized beam.

different from the A_1 peak position. Another possible reason which can lead to the enhancement of the C *K*-edge XMCD signals is the multiple scattering effect caused by the spin-polarized neighbouring atoms.[29] However, the calculations based on the multiple scattering of photoelectrons which come out from absorbing atoms fail to explain the XMCD intensity even if the magnetic moment of the Ni atoms near the interface and that of the C atoms (0.05–0.25 μ_B per C atom)[7,21,24] are taken into account. It is therefore most likely that the spin polarization and also the SOI enhancement are induced in graphene through the π–d hybridization as judged from the A_1 and A_2 peaks. This conclusion is in good agreement with the theoretical study.[30] The small XMCD signals located near the A_3 peak might be responsible for the non-zero spin polarization of the σ^* states considering a moderate SOI strength[27] or the multiple scattering effect.

Further, the direction of the spin polarization in graphene is estimated from the intensities of the C *K*-edge XMCD at $\alpha = 30°$ and $\alpha = 60°$. The relative magnitude of the orbital magnetic moment along α can be given as the ratio (R) of the integral intensity of the XAS and XMCD peaks ($I_{xmcd}(\alpha)/I_{xas}(\alpha)$), which is analogous to the case of the $L_{2,3}$-edge XMCD. A reliable estimation of R can be performed only for the A_1 peak region because of the weak XMCD signals for the other peaks. The value of R is estimated to be 0.7 as follows;

$$R = (I_{xmcd}(30°)/I_{xas}(30°))/(I_{xmcd}(60°)/I_{xas}(60°)),$$

where the XAS and XMCD intensities in the corresponding energy region are calculated for the curve-fit results with a Gaussian line-shape and for the raw data, respectively. This ratio is close to the ratio of $M'_{total}(30°)$ to $M'_{total}(60°)$ (that is 0.6) for Ni under the small probing depth of $\lambda_p = 0.4$ nm. This means that the π^* states of graphene is out-of-plane spin-polarized along the spin polarization direction of the Ni atomic layers adjacent to the interface. So far, the interface-related PMA is known for the multilayers comprising of FMs and nonmagnetic metals and has been discussed in connection with the effects of the hybridization and the lattice strain on the anisotropy of the orbital magnetic moment.[31] The latter, however, would not play an essential role in the present system because of the small lattice mismatch at the graphene/Ni(111) interface. Although further theoretical investigation is required to clarify the detailed mechanism, it is surmised that the interface PMA in the SLG/Ni(111) thin film is mainly caused by the anisotropic change in the orbital magnetic moment induced by the π–d hybridization at the graphene/Ni(111) interface.

Conclusions

In summary, the interface spin-polarized electronic structures in the SLG/Ni(111) thin film are explored by means of depth-resolved XAS and XMCD spectroscopy with atomic layer resolution. This approach leads to the finding that the SLG/Ni(111) thin film undergoes a change of the spin orientation from in-plane to out-of-plane across the graphene/Ni(111) interface; that is, on the Ni(111) thin film side, the spin polarization direction changes from in-plane to out-of-plane toward the interface with the total magnetic moment decrease, and, on the SLG side, the out-of-plane spin polarization as well as the increase of the SOI strength are induced in the π^* states. The interface PMA as in the present study could disturb the spin valve operation of graphene devices with conventional FM electrodes with in-plane magnetization. The present study highlights the importance of the design of the interface spin-polarized electronic structures at the atomic layer level to control the spin injection and for the development of graphene-based spintronics.

Acknowledgements

This work has been performed under the approval of the Photon Factory Program Advisory Committee (proposal no. 2010G664 and 2011G636). The present research was partly supported by the Grant-in-Aid for Scientific Research (Grant no. 22740206, 22760033 and 24360266) from MEXT of Japan. We appreciate ASRC and Molecular Spintronics Group for the cooperation and fruitful discussions.

Notes and references

1 A. K. Geim and K. S. Novoselov, *Nat. Mater.*, 2007, **6**, 183.
2 N. Tombros, C. Jozsa, M. Popinciuc, H. T. Jonkman and B. J. van Wees, *Nature*, 2007, **448**, 571.
3 V. M. Karpan, G. Giovannetti, P. A. Khomyakov, M. Talanana, A. A. Starikov, M. Zwierzycki, J. van den Brink, G. Brocks and P. J. Kelly, *Phys. Rev. Lett.*, 2007, **99**, 176602.
4 E. W. Hill, A. K. Geim, K. Novoselov, F. Schedin and P. Blake, *IEEE Trans. Magn.*, 2006, **42**, 2694.

5 M. Nishioka and A. M. Goldman, *Appl. Phys. Lett.*, 2007, **90**, 252505.
6 H. Goto, A. Kanda, T. Sato, S. Tanaka, Y. Ootuka, S. Odaka, H. Miyazaki, K. Tsukagoshi and Y. Aoyagi, *Appl. Phys. Lett.*, 2008, **92**, 212110.
7 M. Ohishi, M. Shiraishi, R. Nouchi, T. Nozaki, T. Shinjo and Y. Suzuki, *Jpn. J. Appl. Phys.*, 2007, **46**, L605.
8 M. Weser, Y. Rehder, K. Horn, M. Sicot, M. Fonin, A. B. Preobrajenski, E. N. Voloshina, E. Goering and Yu. S. Dedkov, *Appl. Phys. Lett.*, 2010, **96**, 012504.
9 K. Amemiya, *Phys. Chem. Phys. Chem.*, 2012, **14**, 10477.
10 K. Amemiya, S. Kitagawa, D. Matsumura, H. Abe, T. Ohta and T. Yokoyama, *Appl. Phys. Lett.*, 2004, **84**, 936.
11 S. Entani, Y. Matsumoto, M. Ohtomo, P. V. Avramov, H. Naramoto and S. Sakai, *J. Appl. Phys.*, 2012, **111**, 064324.
12 D. A. Fischer, R. M. Wentzcovitch, R. G. Carr, A. Continenza and A. J. Freeman, *Phys. Rev. B*, 1991, **44**, 1427.
13 G. Bertoni, L. Calmels, A. Altibelli and V. Serin, *Phys. Rev. B*, 2005, **71**, 075402.
14 P. Skytt, P. Glans, D. C. Mancini, J.-H. Guo, N. Wassdahl, J. Nordgren and Y. Ma, *Phys. Rev. B*, 1994, **50**, 10457.
15 B. J. Schultz, C. Jaye, P. S. Lysaght, D. A. Fischer, D. Prendergast and S. Banerjee, *Chem. Sci.*, 2013, **4**, 494.
16 H. Amara, S. Latil, V. Meunier, Ph. Lambin and J.-C. Charlier, *Phys. Rev. B*, 2007, **76**, 115423.
17 M. L. Ng, R. Balog, L. Hornekær, A. B. Preobrajenski, N. A. Vinogradov, N. Mårtensson and K. Schulte, *J. Phys. Chem. C*, 2010, **114**, 18559.
18 A. I. Nesvizhskii, A. L. Ankudinov, J. J. Rehr and K. Baberschke, *Phys. Rev. B*, 2000, **62**, 15295.
19 B. T. Thole, P. Carra, F. Sette and G. van der Laan, *Phys. Rev. Lett.*, 1992, **68**, 1943.
20 P. Carra, B. T. Thole, M. Altarelli and X. Wang, *Phys. Rev. Lett.*, 1993, **70**, 694.
21 G. Y. Guo, W. M. Temmerman and H. Ebert, *Physica B*, 1991, **172**, 61.
22 S. J. Gong, Z. Y. Li, Z. Q. Yang, C. Gong, C.-G. Duan and J. H. Chu, *J. Appl. Phys.*, 2011, **110**, 043704.
23 P. V. Avramov, A. Kuzukov, S. Sakai, M. Ohtomo, S. Entani, Y. Matsumoto, H. Naramoto and N. S. Eleseeva, *J. Appl. Phys.*, 2012, **112**, 114303.
24 T. Abtew, B.-C. Shih, S. Banerjee and P. Zhang, *Nanoscale*, 2013, **5**, 1902.
25 J. Igarashi and K. Hirai, *Phys. Rev. B*, 1994, **50**, 17820.
26 D. Huertas-Hernando, F. Guinea and A. Brataas, *Phys. Rev. B*, 2006, **74**, 155426.
27 Y. Yao, F. Ye, X. L. Qi, S. C. Zhang and Z. Fang, *Phys. Rev. B*, 2007, **75**, 041401R.
28 V. L. Joseph Joly, M. Kiguchi, S.-J. Hao, K. Takai, T. Enoki, R. Sumii, K. Amemiya, H. Muramatsu, T. Hayashi, Y. A. Kim, M. Endo, J. Campos-Delgado, F. López-Urías, A. Botello-Méndez, H. Terrones, B. Terrones and M. S. Dresselhaus, *Phys. Rev. B*, 2010, **81**, 245428.
29 T. Fujikawa and S. Nagamatsu, *J. Electron Spectrosc. Relat. Phenom.*, 2003, **129**, 55.
30 Z. Y. Li, Z. Q. Yang, S. Qiao, J. Hu and R. Q. Wu, *J. Phys.: Condens. Matter*, 2011, **23**, 225502.
31 K. Kyuno, J.-G. Ha, R. Yamamoto and S. Asano, *J. Appl. Phys.*, 1996, **79**, 7084.